

# Crystal growth of Hg<sub>2</sub>Cl<sub>2</sub> and Hg<sub>2</sub>Br<sub>2</sub> single crystals by Physical Vapor Transport

Joo-Soo Kim, Sudhir B. Trivedi, Jolanta Soos, Neelam Gupta\*, and Witold Palosz<sup>#</sup>

Brimrose Corporation of America, 19 Loveton Circle, Sparks, Md 21152-9201

\* U.S. Army Research Laboratory, AMSRD-ARL-SE-EE, Adelphi, Md 20783-1197

## Abstract

Large crystals of Hg<sub>2</sub>Cl<sub>2</sub> and Hg<sub>2</sub>Br<sub>2</sub> (48 mm in diameter, up to 600g in weight) have been grown by Physical Vapor Transport (PVT) technique in closed ampoules in vertical configuration without contact with the ampoule walls. The starting materials have been pre-purified by resublimation. Seed selection has been accomplished by having a narrow tubing at the tip of the growth ampoule. Thermochemical analysis of the system is done and discussed. The grown crystals show good transparency and good crystallographic quality. An acousto-optic modulator built from the Hg<sub>2</sub>Cl<sub>2</sub> crystal showed good performance consistent with predicted device parameters.

## 1. Introduction

Acousto-optic (AO) bulk devices, like acousto-optic tunable filters (AOTF) and acousto optic modulators (AOM), are used in a variety of military, space, and commercial applications [1 - 5], e.g. for detection of targets, backgrounds, and stand-off chemical and biological agents [6 - 8]. AO devices are solid-state RF tunable devices that contain no moving parts and are compact, rugged, and highly efficient. High efficiency translates directly into lower operating power, higher sensitivity, and faster data acquisition. AO devices have also high repeatability, can be easily self-calibrated, and can be computer controlled.

In the area of AO material and device development, there are two wavelength regions that still require a development of suitable materials: the deep UV region (down to 190 nm), and the long wavelength infrared (LWIR) region of the atmospheric transmission window (8 - 12 μm). In this paper, we deal with the development of materials for the LWIR region.

The efficiency of AO materials is characterized by the figure of merit:

$$M_2 = \frac{n_i^3 n_d^3 p^2}{\rho V^3}, \quad (1)$$

where  $P_a$  is the acoustic power,  $H_T$  and  $L_T$  are the height and length of the transducer, respectively,  $L$  is the AO interaction length,  $\lambda_0$  is the wavelength of the diffracted light,  $n_i$  and  $n_d$  are, respectively, the refractive index of the incident and diffracted light,  $p$  is the effective photoelastic coefficient,  $\rho$  is the density of the AO material, and  $V$  is the acoustic velocity. In order to have high  $M_2$  the material should offer: (a), high photoelastic coefficient  $p$ , (b), high refractive indices  $n_i$ , and  $n_d$ , and (c), slow acoustic velocity  $V$ . Table 1 lists the key properties of the best AO materials which can be used in the LWIR region. Of those, Tellurium has the highest figure of merit but its narrow bandgap leads to high absorption by thermally activated charge carriers. It is also mechanically fragile and prone to damage. Thallium arsenide-selenide (TAS) has a high figure of merit and can be grown in large, high quality boules [11], but the material is very toxic and requires careful handling procedures and specialized materials processing facilities. However, currently there is no other technologically matured and commercially available material at reasonable price for AO applications in the 8 - 12 μm wavelength range. Some 20 years ago mercurous halides were identified as a new class of promising acousto-optic materials [12 - 13]. Among them, mercurous chloride and bromide are the most suitable for filtering in the LWIR region. Hg<sub>2</sub>Cl<sub>2</sub> crystal is strongly birefringent, with extremely slow shear wave acoustic velocity along the <110> direction. These properties are attributed to the strong anisotropy of the lattice field and the nature of the Hg<sup>+</sup> ion. As seen in Table 1, Hg<sub>2</sub>Cl<sub>2</sub> has high refractive indices, low acoustic attenuation, and  $M_2$  comparable to that of TeO<sub>2</sub> in the slow (shear) acoustic mode. The presence of the shear acoustic mode enables birefringent AO interaction which, in turn, allows non-collinear non-critical phase matching. Such a non-collinear AOTF has a large angular aperture offering high throughput that is vital for imaging spectrometers. Also, the diffracted beam is separated from the undiffracted beam by an angle, so

---

<sup>#</sup> corresponding author: wpalosz@brimrose.com

there is no need to use polarizers (the beams have different polarization planes). Since the separation angle is proportional to  $\Delta n \equiv n_e - n_o$ , the strong birefringence in these materials results in a large separation angle and hence a large acceptance angle.  $\text{Hg}_2\text{Cl}_2$  crystals are also capable of withstanding large optical power densities.

Table 1. Relevant properties of AO materials. (References given in the first column concern all properties except for those with own references.)

| Material                              | Transmission range [ $\mu\text{m}$ ] | $M_2$ [ $10^{-15} \text{ s}^3/\text{kg}$ ] | $n_o$     | $n_e$     | Mode and propagation direction | Velocity [m/s] | Density $\text{g}/\text{cm}^3$ | Acoustic Attenuation [ $\text{dB } \mu\text{s}^{-1} \text{ GHz}^{-2}$ ] |
|---------------------------------------|--------------------------------------|--|-----------|-----------|--------------------------------|----------------|--------------------------------|---|
| Te [3]                                | 4.0 - 20.0                           | 4,400 [15]                                 | 4.79      | 6.24      | L [11-20]                      | 2,300          | 6.25 [16]                      |   |
| $\text{Tl}_3\text{AsSe}_3$ (TAS) [14] | 1.26 - 13.0                          | 2,900 [3]                                  | 3.42 [17] | 3.23 [17] | L [100]                        | 2,050          | 7.83                           | 14.0  |
| $\text{Hg}_2\text{Cl}_2$ [14]         | 0.38 - 28                            | 509<br>1060                                | 1.96 [3]  | 2.62 [3]  | L [100]<br>S [110]             | 1,620<br>347   | 7.18                           | 8.0   |
| $\text{Hg}_2\text{Br}_2$ [10]         | 0.4 - 30                             | 2,600                                      | 2.12      | 2.98      | S [110]                        | 273            | 7.307                          | 11.8  |

Mercurous bromide ( $\text{Hg}_2\text{Br}_2$ ), another of the mercurous halides, may also be suitable for LWIR acousto-optic applications [18]. The optical transparency range, 0.4 to 30 microns, extends even further than that of  $\text{Hg}_2\text{Cl}_2$ . Furthermore,  $\text{Hg}_2\text{Br}_2$  is highly birefringent: about 25% in the infrared and about 40% in the visible. No other known material has such a large value of birefringence, which is extremely important in the design of optical devices.  $\text{Hg}_2\text{Br}_2$  has high refractive indices and an even lower acoustic attenuation compared to  $\text{Hg}_2\text{Cl}_2$ . A value of  $M_2$  for  $\text{Hg}_2\text{Br}_2$  is about 2.5 times that of  $\text{Hg}_2\text{Cl}_2$  and comparable to TAS [10], although this figure has not been measured experimentally [18].

Thus,  $\text{Hg}_2\text{Cl}_2$  and  $\text{Hg}_2\text{Br}_2$  are the best materials for building AO devices including those for an imaging system for operation in the LWIR region. However, the potential of these materials has not been exploited for at least two reasons: (1), a lack of easy commercial availability of device quality crystals (it is very difficult to acquire high quality material, and standardized growth and processing techniques for obtaining device quality crystals have not been developed yet), and (2), lack of standardized device processing techniques (the mercurous halides are very corrosive to the metallic films that are deposited on the crystals for bonding purposes, therefore device fabrication is not trivial). Application of the halides for some devices has already been demonstrated [13, 19 - 22].

$\text{Hg}_2\text{Cl}_2$  and  $\text{Hg}_2\text{Br}_2$  are extremely difficult to purify because in the presence of trace impurities they very easily oxidize. Also, the halides are almost completely insoluble in most solvents, inhibiting growth by solution techniques. Solidification techniques generally fail because the material easily decomposes into Hg and  $\text{HgX}_2$  before melting. Thus,  $\text{Hg}_2\text{Cl}_2$  and  $\text{Hg}_2\text{Br}_2$  crystals are typically grown by the physical vapor transport technique. However, during the early stages of crystal growth of mercurous halides via PVT, defects such as inclusions, nonstoichiometry, mosaic structure, growth rings, and striations are frequently observed. Thus, the current work on the crystal growth of  $\text{Hg}_2\text{Cl}_2$  and  $\text{Hg}_2\text{Br}_2$  has generally focused on understanding the purification and growth mechanisms, increasing the homogeneity and producing crystals that are large enough to fabricate a device. This paper discusses the thermochemistry of the system, describes the purification and crystal growth techniques that we have developed, and presents our results on the optical characterization of the crystals and AOM device fabricated based on  $\text{Hg}_2\text{Cl}_2$ .

## 2. Theoretical calculations.

Thermochemical calculations have been made assuming a presence of the mercurous halide and mercury oxide (as the key impurity) solids, and of gaseous species:  $\text{HgX}_2$ , Hg,  $\text{HgX}$ ,  $\text{HgO}$ ,  $\text{O}_2$ , and  $\text{X}_2$ . Thermochemical data for the calculations were taken from refs. [24, 25]. The results of the calculations of equilibrium partial pressures in the  $\text{Hg}_2\text{Cl}_2+\text{HgO}$  system are shown in Fig. 1a. The chloride vaporizes primarily dissociatively with formation of mercury and  $\text{HgCl}_2$  vapors; formation of  $\text{HgCl}$  and  $\text{Cl}_2$  species is negligible. The pressure of  $\text{HgCl}_2$  in the temperature range of interest is lower than that over condensed phase of  $\text{HgCl}_2$ , therefore no mercury chloride should precipitate in the system. The calculations show also a high equilibrium pressure of oxygen and  $\text{HgO}$  implying a significant transport of oxygen concurrent with the chloride during resublimation. Those results are discussed later in connection with our experimental results.

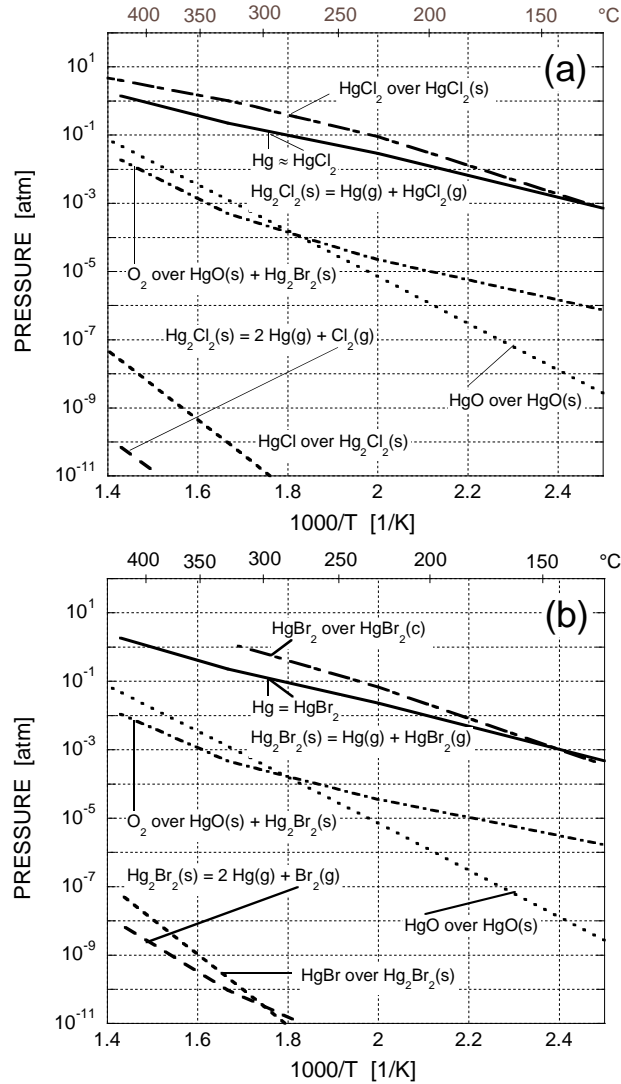


Fig. 1 Partial pressures in the  $(\text{Hg}_2\text{X}_2 + \text{HgO})$  system. (a),  $\text{Hg}_2\text{Cl}_2$ ; (b),  $\text{Hg}_2\text{Br}_2$ .

Similar results as for the chloride were obtained for mercurous bromide (Fig. 1b): vaporization is dominated by formation of mercury(2) bromide, but no precipitation of  $\text{HgBr}_2$  is expected. Also, oxygen-bearing species have partial pressure only 2 - 3 orders of magnitude lower than that of the bromide.

### 3. Materials preparation and crystal growth

Commercially available 99.5%  $\text{Hg}_2\text{Cl}_2$  and 99.9%  $\text{Hg}_2\text{Br}_2$  (each from a different vendor) were used as the starting materials (powders). About 500 g of a given material is loaded into one chamber of pre-cleaned and outgassed purification ampoule (Pyrex). Purification process was similar to that reported in ref. [23]. After outgassing the material at the temperature in the range of 100 - 120°C in vacuum to less than  $10^{-5}$  Torr, the ampoule is sealed off and placed in the furnace as shown schematically in Fig. 2a. The source and sublimate chambers are placed in pre-selected temperature gradient and the material is resublimed. After several such resublimations the required purity is achieved. After the first resublimation near all impurities present originally in the commercial material are left behind (Figs. 2 b and 2c). The dominant impurity in the chloride residue was found to be oxygen, carbon, silica, and chlorine, plus several metal impurities (apparently carbon being responsible for the black color of the residue). The bromide residue was mostly mercury and oxygen (plus several metal impurities and bromine), and the orange color of the residue is apparently due to  $\text{HgO}$ .

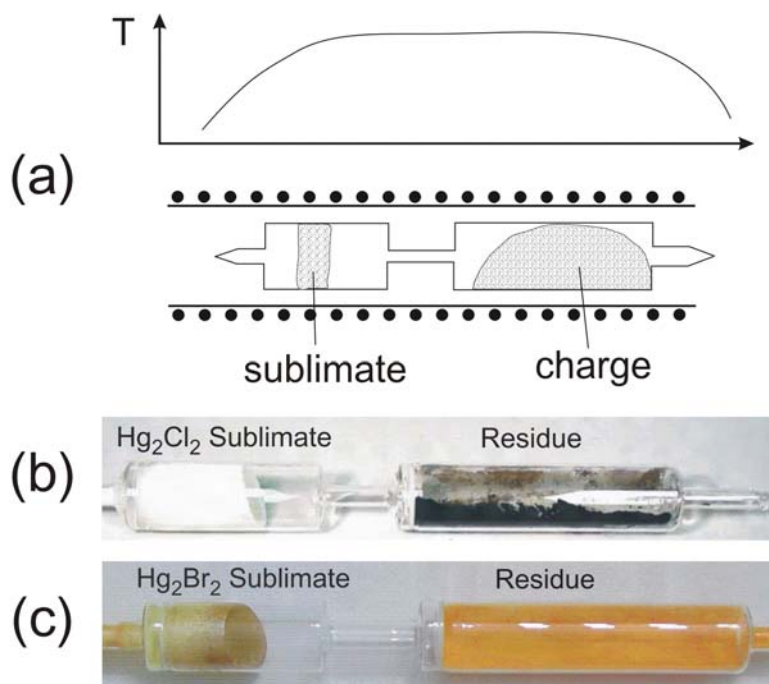


Fig. 2 Materials purification. (a), schematic of the purification system; (b, c), purification ampoules after the first resublimation.

400 - 600g of the purified starting material is loaded into the growth ampoule made of fused silica (inner diameter of 48 mm). The ampoule has a narrow channel in the growth chamber for nucleation and seed selection for subsequent crystal growth (Fig. 3). The growth chamber is separated from the source chamber. The source material in the ampoule is baked and sealed off under vacuum ( $< 10^{-5}$  Torr). The ampoule with the source is placed in the transparent growth furnace shown in Fig. 3. Initially the ampoule is under inverse temperature gradient to clean the growth chamber from undesired seed crystallites. During growth the source temperature is between 320 and 380°C, the crystal growth is carried out in the temperature gradient in the range of 5 - 25°C. Seed development and selection is accomplished with a proper manipulation of the position of the ampoule. After the seed is developed and extends into the tapered part of the ampoule the growth rate is established at about 5 mm a day. Fig. 4 illustrates consecutive stages of the growth process. Seed self-selection process leads usually to growth approximately in the [001] direction. After growth is complete the crystal is cooled down to room temperature over a period of a few days. The ampoule with Hg<sub>2</sub>Br<sub>2</sub> crystal after growth is shown in Fig. 3.

Based on our thermochemical calculations (Figs. 1a and 1b) (and assuming that the thermochemical data used for the calculations are reasonably accurate) oxygen might be expected to be a serious problem in crystal growth of the halides by PVT. The oxygen may be present due to oxidation of the materials in the air as well as a consequence of the synthesis process. Our crystals do not contain any apparent amount of oxygen, and no traces of HgO have been found in the crystallization zone. No traces of mercury and, thus, of HgO have been found in the residue left after Hg<sub>2</sub>Cl<sub>2</sub> purification, what indicates a low level of oxygen in the starting material. However, a presence of considerable quantity of mercury oxide in the Hg<sub>2</sub>Br<sub>2</sub> residue is quite obvious. Still, no trace of HgO phase in the crystal zone have been found. We don't have any immediate explanation for this observation, although we venture into the following potential scenario:

Based on the calculated partial pressures, growth parameters, and the system geometry, and using diffusion equation, we have estimated that the amount of residual gases in the system (which limits the mass transport rate) is on the order of 0.01 atm. Typical residual gas found in crystal growth systems in outgassed silica glass ampoule is carbon monoxide (usually at about 1 Torr pressure) generated from residual oxides and carbon in the system [26]. However, the reaction between graphite impurities and residual oxides may be expected to be kinetically handicapped at low temperatures used in our processes. On the other hand, based on our thermochemical calculations, the pressure of oxygen and HgO in our systems is on the same order as that estimated for residual gases present in the ampoule. Such situation might take place if precipitation of HgO from the vapor is kinetically suppressed and the magnitude of the stationary layer of (O<sub>2</sub>(g) + HgO(g)) determines the mass transport rate in the

system. Since only 1 - 2 mg of oxygen is sufficient to account for 0.01 atm pressure in the ampoule, this mechanism of mass transport rate limitations might dominate both in ampoule with  $\text{Hg}_2\text{Br}_2$  as well as with  $\text{Hg}_2\text{Cl}_2$  (where no apparent presence of  $\text{HgO}$  could be confirmed).

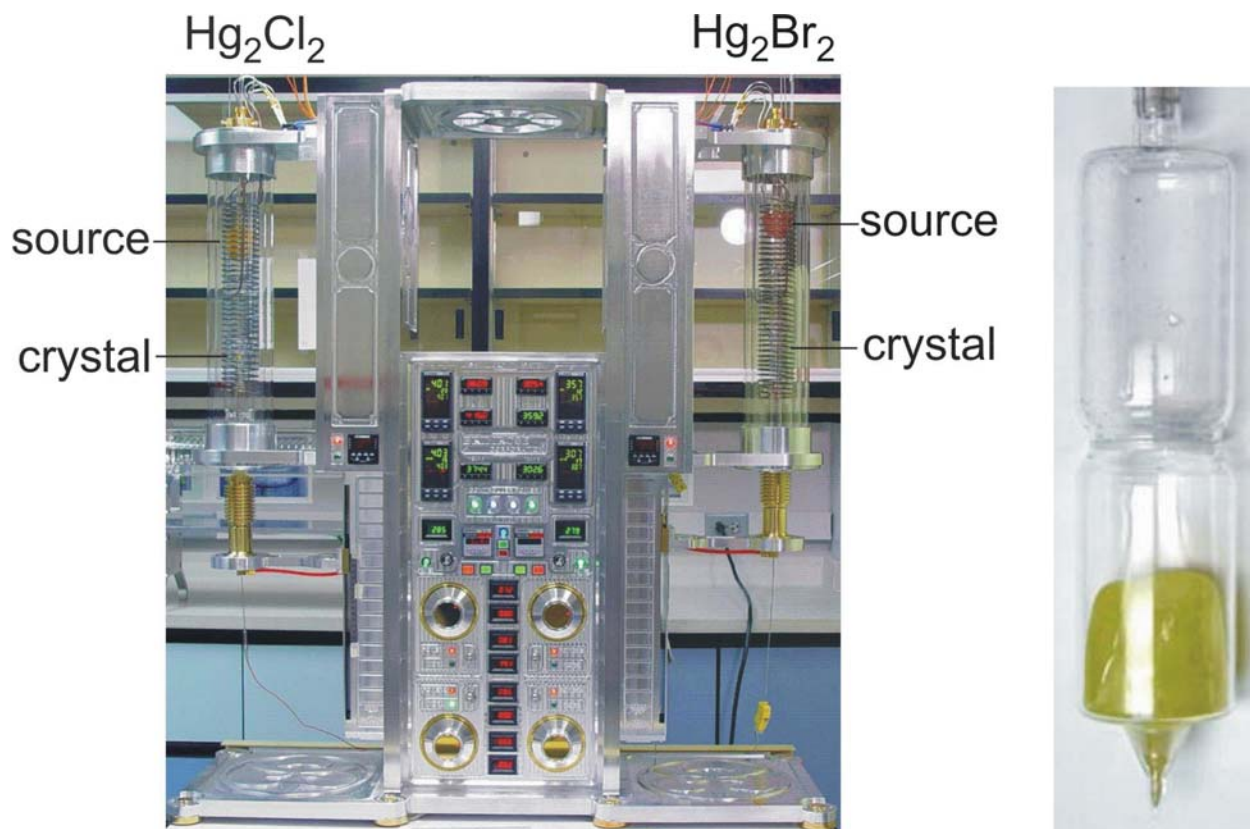


Fig. 3 Crystal growth furnace (at the early stage of growth) and ampoule with  $\text{Hg}_2\text{Br}_2$  after growth.

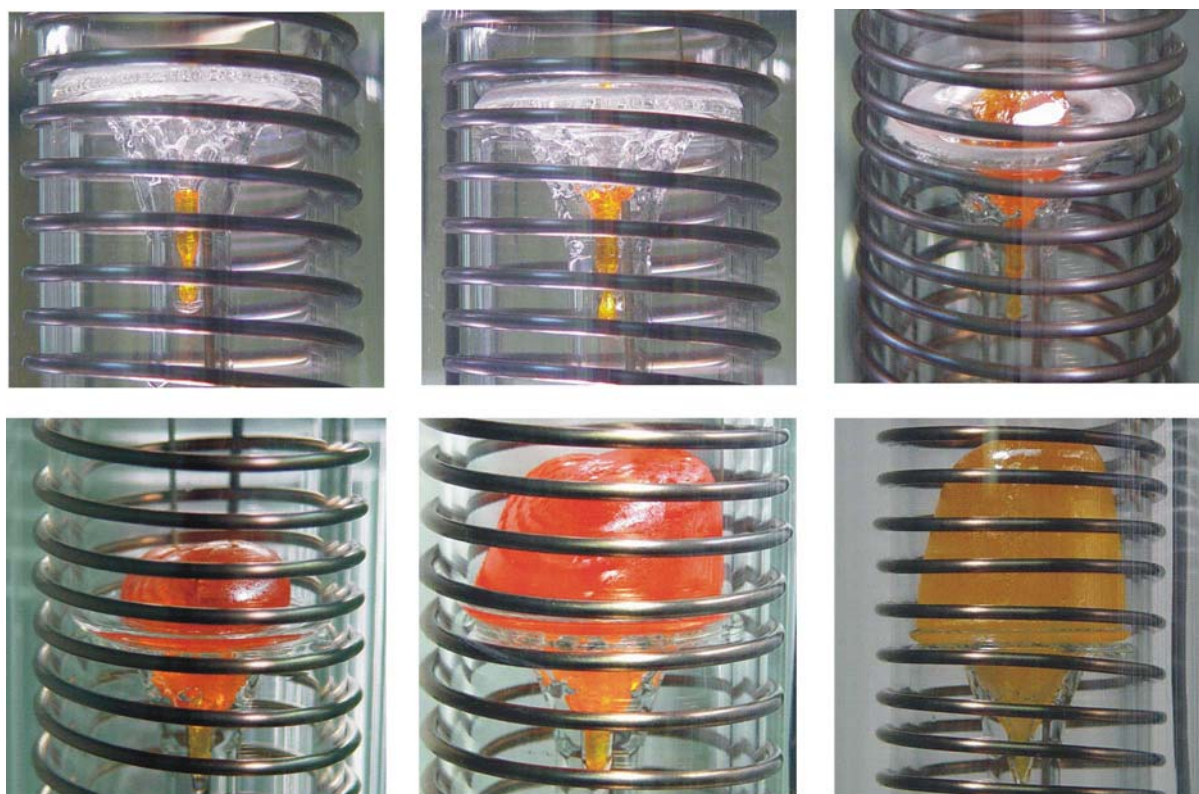


Fig. 4 Consecutive stages of growth of  $\text{Hg}_2\text{Br}_2$  crystal.

#### 4. Crystals

The grown crystals and cut out samples of  $\text{Hg}_2\text{Cl}_2$  and  $\text{Hg}_2\text{Br}_2$  are shown in Figs. 5a and 5b, respectively. The chloride and bromide crystals are singlecrystalline, with good transparency and few defects.  $\text{Hg}_2\text{Br}_2$  exhibits a presence of some twins. The  $\text{Hg}_2\text{Cl}_2$  sample cut in the (110) plane shown in Fig. 5a demonstrates birefringence of the material. Laue *X-ray* diffraction pattern (Fig. 6,  $\text{Hg}_2\text{Cl}_2$  crystal) shows good quality of the crystal. Fig. 7 shows the transmission curves of the grown halides (the measurements were taken on samples without antireflection coating thus the transmission is relatively low). The smooth transmission curves in the wide spectral range reflect high quality of the crystals.

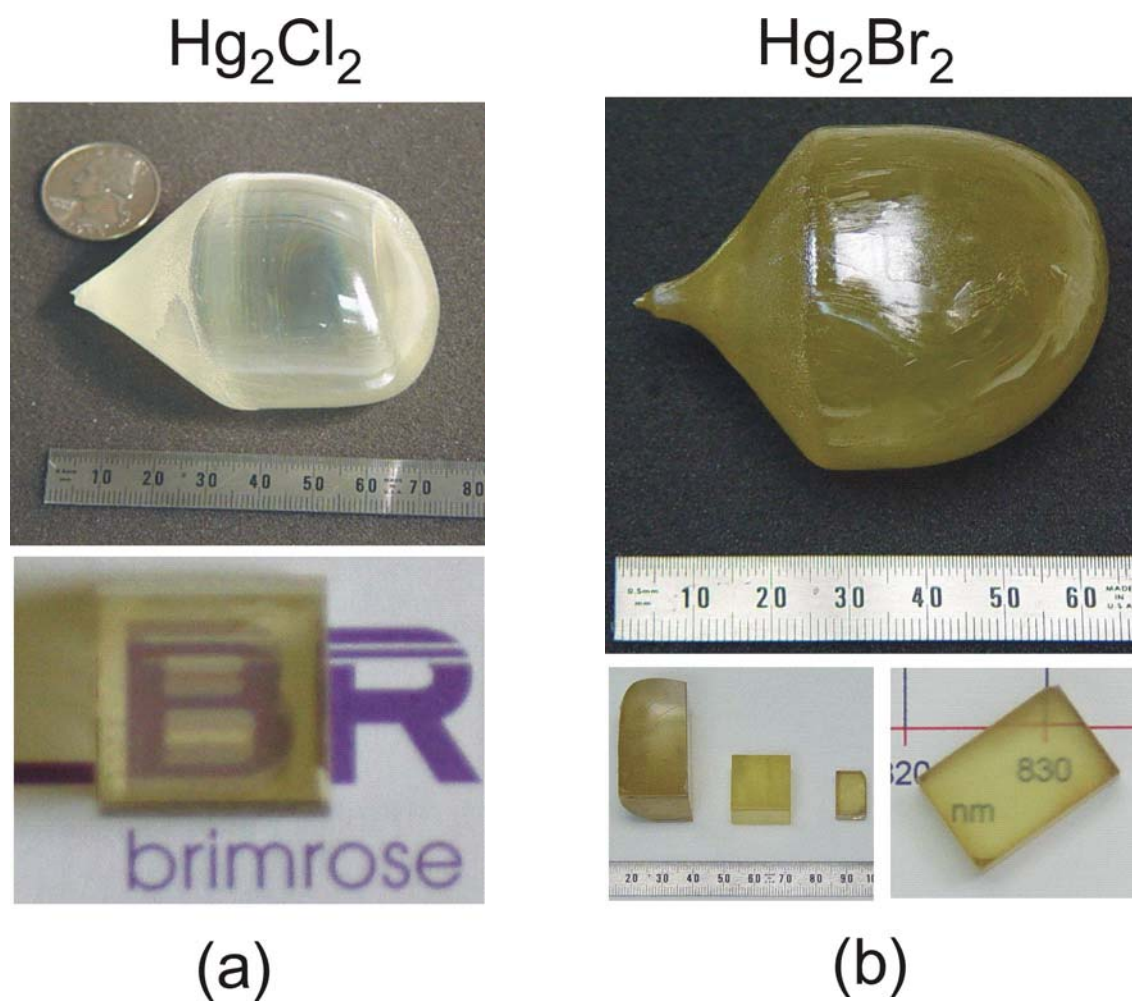


Fig. 5 As-grown crystals and cut-out samples. (a),  $\text{Hg}_2\text{Cl}_2$ ; (b),  $\text{Hg}_2\text{Br}_2$ .

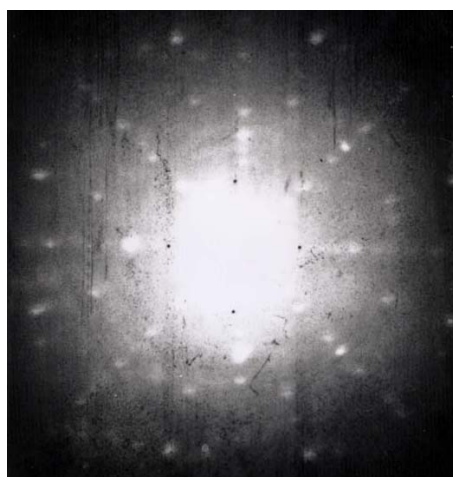


Fig. 6 Laue *X-ray* diffraction pattern of  $\text{Hg}_2\text{Cl}_2$  crystal.

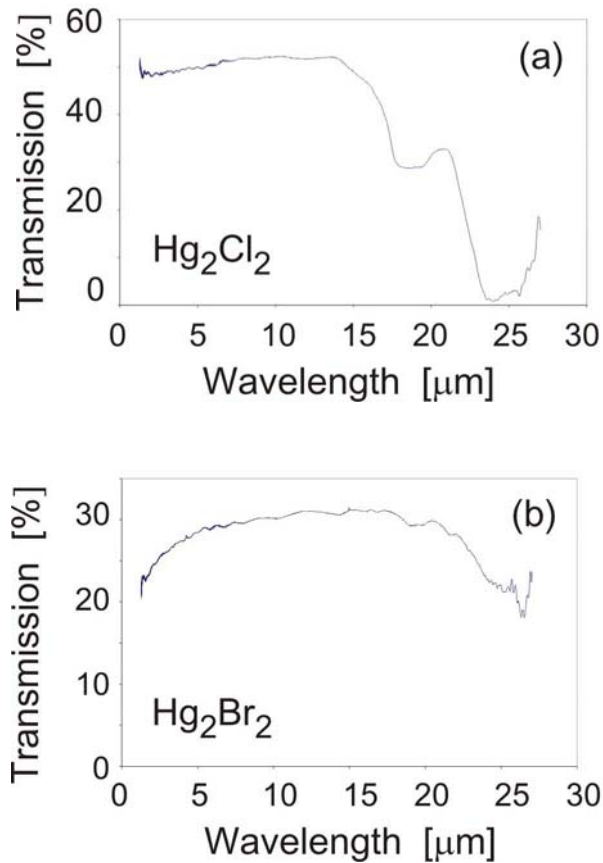


Fig. 7 Transmission curves of the crystals.

## 5. AOM Fabrication and Testing

An acousto-optic modulator (the Bragg cell) uses the acousto-optic effect to modify light using sound waves. A piezoelectric transducer attached to a birefringent transparent material creates sound waves in the medium which cause a (running) periodic density changes. The incoming light scatters off the resulting periodic inhomogeneities in the material density and leads to interference effects. The properties of the light passing through the AOM can be modified in terms of direction, intensity, frequency, phase, and polarization. An acousto-optic modulator operating in longitudinal mode and fabricated from our  $\text{Hg}_2\text{Cl}_2$  crystals is shown in Fig. 8.

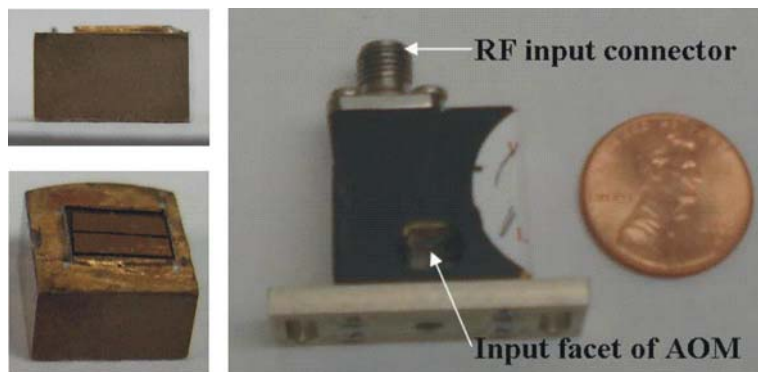


Fig. 8 The crystal with attached transducer (left) and the final device.

A 633 nm HeNe laser was used to test the AOM. The device was placed between a pair of polarizer and analyzer as shown in Fig. 9. The polarizer setting was vertical, parallel to the laser polarization and the analyzer was rotated to get the maximum intensity of the diffracted light. The AOM was designed to operate with a center frequency of 10

MHz. A 1W RF signal was applied to the AOM. When the RF signal was applied, diffracted spots were observed. Fig. 10 shows the diffraction image observed at 9.5 MHz: one non-diffracted (zero order) and two first order spots. The device operated in the Raman-Nath mode. The deflection efficiency was 20%. When the screen was placed at 142.5 cm away from the AOM, the spacing between adjacent spots was 0.5 cm. This gives the measured angular spacing between the first order diffracted beam and the zero order beam (or the incident beam) equal to 3.5 mrad, in a very close agreement with the theoretical value of 3.7 mrad.

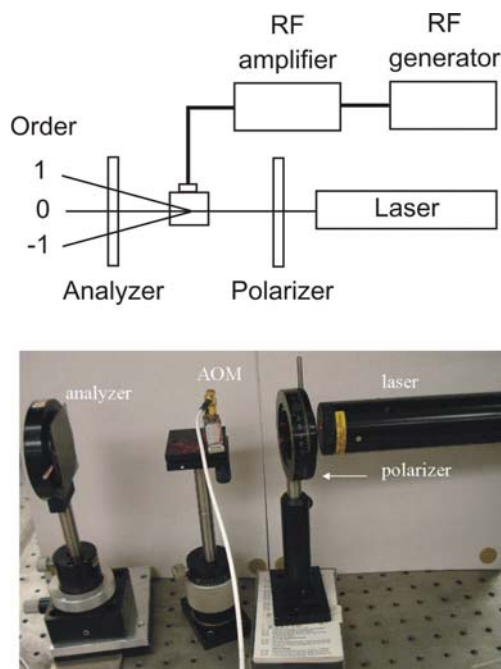


Fig. 9 Experimental set up for AOM characterization.

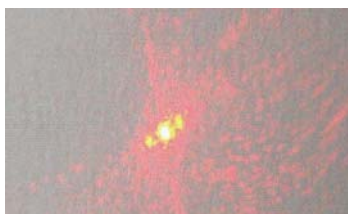


Fig. 10 A photograph of diffraction image from AOM.

## 6. Summary

High quality, transparent crystals of mercurous chloride and mercurous bromide of 48 mm in diameter and weighing 400 - 600 g were grown using unseeded PVT technique. The crystals grew without contact with the side walls of the ampoule. They show high transparency in a wide spectrum range and good crystallographic quality. An acousto-optic modulator was fabricated using our  $\text{Hg}_2\text{Cl}_2$  crystal. The device operated as expected.

## Acknowledgements

The work was supported by U.S. Army Research Laboratory, contract W911QX-06-C-0074.

## References

1. O. Cakmakci and J. Rolland, J. Display Technology 2 (2006) 199.
2. R.J. Thompson, J.M. Kohel, J.R. Kellogg, D.C. Aveline, L. Maleki, and N. Yu, NASA Science Conference (2007).
3. N. Gupta, SPIE Proceedings, vol. 5953 (2005) 1.

4. M.L. Nischan, R.M. Joseph, J.C. Libby, and J.P.Kerekes, *Lincoln Lab. Journal* 14 (2003) 131.
5. K.A. Bakeev, Ed., *Process Analytical Technology: Spectroscopic Tools and Implementation Strategies for the Chemical and Pharmaceutical Industries* (Blackwell Publishing, 2005).
6. N. Gupta, R. Dahmani, and S. Choy, *Opt. Eng.* 41 (2002) 1,033.
7. N. Gupta, L. Denes, M. Gottlieb, D. Suhre, B. Kaminsky, and P. Metes, *Appl. Opt.* 40 (2001) 6,626.
8. D.R. Suhre, L.H. Taylor, N.B. Singh, and W.R. Rosch, *SPIE Proc.* vol. 3584 (1999) 142.
9. I.C. Chang, *IEEE Trans. Sonics and Ultrasonics*, vol. SU-23 (1976) 2.
10. D.J. Knuteson, N.B. Singh, M. Gottlieb, D. Suhre, N. Gupta, A. Berghmans, D. Kahler, B. Wagner, J. Hawkins, *Opt. Eng.* 46 (2007).
11. J. Xu and R. Stroud, *Acousto-Optic Devices* (Wiley, New York, 1992).
12. M. Gottlieb, A.P. Goutzoulis, and N.B. Singh, *Appl. Optics* 26 (1987) 4,681.
13. N.B. Singh, M. Gottlieb, and A. Goutzoulis, *J. Crystal Growth* 82 (1987) 274.
14. *Handbook of Optics*, Ed. M. Bass (McGraw Hill, 1995).
15. A. Yariv, *Quantum Electronics* (Wiley, 1988).
16. *Handbook of Chemistry and Physics*, 72th Edition, Ed. D.R. Lide (CRC Press, 1991).
17. *Handbook of Optical Materials*, ed. M.J. Weber (CRC Press, 2002).
18. A. P. Goutzoulis and M. Gottlieb, *Opt. Eng.* 27 (1988) 157.
19. D.J. Knuteson, N.B. Singh, N. Gupta, M. Gottlieb, D. Suhre, A. Berghmans, D. Thomson, D. Kahler, B. Wagner, J. Hawkins, and M. Fitelson, *Proc. SPIE* vol. 5881 (2005).
20. N.B. Singh, D. Suhre, N. Gupta, W. Rosch, and M Gottlieb, *J. Crystal Growth* 225 (2001) 124.
21. A.P. Goutzoulis, M. Gottlieb, and N. B. Singh, *Proc. SPIE* vol. 753 (1987) 29.
22. N.B. Singh, T. Henningsen, D.R.Suhre, W. Rosch, R.H. Hopkins, R. Mazelsky, S.R. Coriell, and W.M.B. Duval, *J. Crystal Growth* 198/199 (1999) 995.
23. N.B. Singh, R.H. Hopkins, R. Mazelsky, and J.J. Conroy, *J. Crystal Growth* 75 (1986) 173.
24. Barin & Knacke, *Thermochemical Properties of Inorganic Substances* (Springer, Berlin, 1974).
25. Barin, Knacke, & Kubashevsky, *Thermochemical Properties of Inorganic Substances, Supplement*, (Springer, Berlin, 1974).
26. W. Palosz, *J. Crystal Growth* 267/3-4 (2004) 484.